⌘ *Author's Choice*

THE JOURNAL OF BIOLOGICAL CHEMISTRY VOL. 285, NO. 15, pp. 11730–11739, April 9, 2010
Printed in the U.S.A.

MutLα and Proliferating Cell Nuclear Antigen Share Binding Sites on MutSβ*[S]

Received for publication, January 14, 2010, and in revised form, February 12, 2010 Published, JBC Papers in Press, February 12, 2010, DOI 10.1074/jbc.M110.104125

Ravi R. Iyer[‡], Anna Pluciennik[‡], Jochen Genschel[‡], Miaw-Sheue Tsai[§], Lorena S. Beese[‡], and Paul Modrich[‡¶1]

From the [‡]Department of Biochemistry and the [¶]Howard Hughes Medical Institute, Duke University Medical Center, Durham, North Carolina 27710 and the [§]Department of Cancer and DNA Damage Responses, Life Sciences Division, Lawrence Berkeley National Laboratory, Berkeley, California 94720

MutSβ (MSH2-MSH3) mediates repair of insertion-deletion heterologies but also triggers triplet repeat expansions that cause neurological diseases. Like other DNA metabolic activities, MutSβ interacts with proliferating cell nuclear antigen (PCNA) via a conserved motif (Q*XX*(L/I)*XX*FF). We demonstrate that MutSβ-PCNA complex formation occurs with an affinity of ~0.1 μM and a preferred stoichiometry of 1:1. However, up to 20% of complexes are multivalent under conditions where MutSβ is in molar excess over PCNA. Conformational studies indicate that the two proteins associate in an end-to-end fashion in solution. Surprisingly, mutation of the PCNA-binding motif of MutSβ not only abolishes PCNA binding, but unlike MutSα, also dramatically attenuates MutSβ-MutLα interaction, MutLα endonuclease activation, and bidirectional mismatch repair. As predicted by these findings, PCNA competes with MutLα for binding to MutSβ, an effect that is blocked by the cell cycle regulator p21[CIP1]. We propose that MutSβ-MutLα interaction is mediated in part by residues ((L/I)SRFF) embedded within the MSH3 PCNA-binding motif. To our knowledge this is the first case where residues important for PCNA binding also mediate interaction with a second protein. These findings also indicate that MutSβ- and MutSα-initiated repair events differ in fundamental ways.

The mammalian mismatch repair system stabilizes the genome by correcting DNA biosynthetic errors, preventing illegitimate recombination events, and participating in the cellular response to certain types of DNA damage (reviewed in Ref. 1–5). Mismatch repair deficiency is the cause of hereditary nonpolyposis colorectal cancer but may also be involved in the development of a subset of sporadic tumors (6).

The human mismatch recognition activities MutSα (MSH2–MSH6) and MutSβ (MSH2 and MSH3) differ in their substrate specificities: MutSα recognizes base-base mismatches and some insertion-deletion (I/D)[2] mismatches, whereas MutSβ predominantly processes I/D substrates (1–5). MutSα is also capable of recognizing certain types of DNA damage and participates in the checkpoint response to such lesions (7), whereas MutSβ is believed to cooperate with the nucleotide excision repair machinery in the repair of interstrand cross-links (8, 9). Thus, there is substantial overlap between the substrates recognized and processed by these two activities, but the determinants that govern whether a particular lesion is processed by MutSα or MutSβ are not known.

Although MutSα and MutSβ are generally regarded as genetic stabilization activities, both heterodimers have been implicated in the production of certain mutations. MutSα participates in the somatic hypermutation phase of immunoglobulin gene affinity maturation (10), and MutSβ is required for the triplet repeat expansions that are responsible for a number of neurodegenerative diseases (11).

Heteroduplex repair reactions initiated by MutSα and MutSβ have been reconstituted in a purified systems that also contain MutLα (MLH1-PMS2), exonuclease 1 (Exo1), RPA (replication protein A), PCNA, RFC, and DNA polymerase δ (12–16). Initiation of repair in the MutSα-dependent system involves activation of a latent endonuclease of MutLα in a reaction that requires a mismatch, MutSα, RFC, PCNA, and ATP (16). Action of the MutLα endonuclease is directed to the heteroduplex strand that contains a pre-existing break and is biased to the distal side of the mismatch to yield a molecule in which the mismatch is bracketed by strand breaks. This multiply incised intermediate serves as substrate for Exo1, which is activated by MutSα in a mismatch-dependent manner, leading to mismatch removal. The ensuing gap is filled by RPA and repaired by DNA polymerase δ in a reaction that also depends on PCNA and RFC. Although a MutSβ-dependent repair reaction has been reconstituted from purified components (15), it is not known whether activation of the MutLα endonuclease occurs in a MutSβ-dependent manner.

Coordination of these activities during the course of repair is presumably mediated by a temporally evolving set of protein-protein and protein-DNA interactions. The most thoroughly studied of the multi-protein assemblies involved in mismatch repair have been the MutSα-MutLα complex that assembles on heteroduplex DNA (17–19) and the MutSα-PCNA complex that has been observed both in solution and on DNA (20, 21). Although the former complex is generally believed to play an important role in the reaction (22), disruption of the MutSα-PCNA interaction confers only a partial mismatch repair defect *in vivo* and *in vitro* (20, 21, 23). Although the MutSβ-

* This work was supported, in whole or in part, by National Institutes of Health Grants R01 GM45190 and P01 CA92584.

⌘ *Author's Choice*—Final version full access.

[S] The on-line version of this article (available at http://www.jbc.org) contains supplemental Table S1 and Figs. S1 and S2.

[1] Investigator of the Howard Hughes Medical Institute. To whom correspondence should be addressed. Tel.: 919-684-2775; Fax: 919-681-7874; E-mail: modrich@biochem.duke.edu.

[2] The abbreviations used are: I/D, insertion-deletion; PCNA, proliferating cell nuclear antigen; RFC, replication factor C; SPRS, surface plasmon resonance spectroscopy; SAXS, small angle x-ray scattering; PIP, PCNA interacting peptide.

PCNA and MutSβ-MutLα complexes have been the subject of only limited study (23–26), yeast strains carrying mutations in the PCNA-binding motif of MSH3 display hypermutability similar to that of MSH3 null mutant (23). Also, little is known regarding the functional significance of the MutSβ-MutLα interaction. We demonstrate here that MutSβ differs from MutSα in the manner that it interacts with PCNA and MutLα.

EXPERIMENTAL PROCEDURES

MutSβ-expressing Baculovirus Constructs—The baculoviral donor plasmid pFastBacDual-MSH2-MSH3 (9) that harbors full-length MSH2 and MSH3 was modified by PCR mutagenesis to yield pFastBacDual-MSH2-MSH3Δ28, which contains intact MSH2 and an N-terminally truncated MSH3 gene encoding amino acids 29–1137 of full-length MSH3 beginning with N-Met (see Fig. 1*A*). A second construct, pFastBacDual-MSH2-MSH3-F27A-F28A harboring MSH3 that contains Phe to Ala amino acid substitutions at positions 27 and 28 (see Fig. 1*A*), was also prepared by PCR mutagenesis of the full-length construct. High titer recombinant baculoviruses were prepared from the expression vectors and used to infect Sf9 cells for protein expression.

DNA Substrates and Proteins—Bacteriophages f1MR72 and f1MR73 were constructed by oligonucleotide mutagenesis of f1MR23 and f1MR24 (27), respectively, resulting in substitution of an EcoRV site for residues 5501–5506 as described for phages f1MR70 and f1MR71 (28). 6,440-bp dinucleotide insertion/deletion heteroduplex DNAs (-TG-) were constructed as described (27) from phages f1MR72 and f1MR73 and contained a site-specific nick in the complementary DNA strand 128 bp 3′ or 5′ to the mismatch as viewed along the shorter path in the circular molecules. The strand break for 5′ -TG- was introduced by cleavage with Sau96I, whereas the strand break in 3′ -TG- was introduced by cleavage with EcoRV (28). Substrates for analyses of DNA-protein assemblies by SPRS were 200 bp in length and were prepared as follows. Primers 5′-CCGCTACACTTGCCAGCGCCA-3′ and 5′-biotin-GTTCAAAAAACCCCAGCTCC-3′ were used to generate 200- and 202-bp PCR products from f1MR23 and f1MR24 (27), respectively. The strands were separated by denaturing high pressure liquid chromatography (29) and reannealed to generate a heteroduplex containing a centrally positioned -TG- loop, or an otherwise identical homoduplex.

MutSβ, MSH2-MSH3Δ28 (referred to as MutSβΔ28), and MSH2-MSH3-F27A-F28A (referred to as MutSβ-F27A-F28A) were prepared from baculovirus-infected Sf9 cells by a procedure essentially identical to that described for native human MutSβ (30). All other proteins were purified as described in the work of Iyer *et al.* (21) and the references listed therein. Concentrations of MutSβ are expressed as heterodimer equivalents using an extinction coefficient of 136,690 M^{-1} cm^{-1} at 280 nm for MutSβ (31).

Analyses of Protein-Protein and Protein-DNA Assemblies—Gel filtration chromatography was performed at 4 °C as described (21). SPRS experiments were done on a Biacore 2000 (17, 21) in a buffer composed of 25 mM HEPES-NaOH, pH 7.5, 150 mM NaCl (unless otherwise indicated), 5 mM $MgCl_2$, 1 mM EDTA, and 0.1 mM dithiothreitol. Streptavidin sensor chips were derivatized with ~200 response units of a 200-bp -TG-I/D heteroduplex or an otherwise identical homoduplex DNA via a 5′ biotin tag.

Far Western analyses were performed by spotting 0.25–4 pmol of the indicated proteins on a nitrocellulose membrane (Protran, Whatman) or by electrophoresing 2 pmol of protein through a 7% SDS-polyacrylamide gel, followed by transfer to nitrocellulose. After incubation in blocking buffer (10 mM Tris-HCl, pH 8.0, 150 mM NaCl, 1 mM EDTA, 0.1% Triton X-100, and 5% milk solids) for 1 h at room temperature, the membrane was incubated overnight at 4 °C with PCNA or MutLα in blocking buffer as indicated, followed by two buffer washes. The presence of bound MutLα or PCNA was detected immunochemically with mouse anti-MLH1 or anti-PCNA antibodies.

Small Angle X-ray Scattering (SAXS) Experiments—SAXS was performed on the Sibyls Beamline 12.3.1 at ALS, Berkeley. The scattering data were collected over a range of protein concentrations (10–50 μM) in a buffer containing 25 mM HEPES-KOH, pH 7.5, 150 mM KCl, 5 mM $MgCl_2$, and 1 mM dithiothreitol, and data analyses were performed as described (21). For SAXS-based stoichiometry measurements, the scattering data were collected for mixtures of PCNA and MutSβ (or MutSβΔ28) in which PCNA concentration was varied (3.3–105 μM) at a fixed concentration of MutSβ (10, 20, or 35 μM) or MutSβΔ28 (10 μM) in the buffer described above. Concentration-normalized scattering data were then used to derive forward scattering intensities $I(0)$ (intensity at $\theta = 0°$) (32). The theoretical $I(0)$ for a protein mixture was estimated as the sum of the expected $I(0)$ contributions of each component of that mixture, the latter property being the product of a mass fraction of the component and the $I(0)$ value corresponding to its molecular mass (supplemental Fig. S2*B*). Because protein concentrations were much higher than the K_d for MutSβ-PCNA interaction (see Fig. 1), the limiting species was assumed to be present only in the $(MutS\beta)_n$-PCNA complex.

Mismatch Repair Assays—Bidirectional mismatch-provoked excision and repair assays were carried out at 37 °C for 30 min by complementation of 100 μg of RL95-2 ($MSH2^{-/-}$) nuclear extracts with recombinant MutSβ as indicated in 10-μl reactions containing 20 mM Tris-HCl, pH 7.6, 110 mM KCl, 5 mM $MgCl_2$, 1 mM reduced glutathione, 1.5 mM adenosine triphosphate, 0.05 mg/ml bovine serum albumin, and a 6440-bp -TG- I/D heteroduplex or homoduplex substrate (2.4 nM) (21). Mismatch repair in extracts was performed in a similar manner, except that the reactions also contained 0.1 mM each of dATP, dTTP, dCTP, and dGTP. Excision was scored by conversion of DNA to a NheI-resistant form (33), and repair was measured by restoration of XcmI sensitivity to the heteroduplex DNA (27). MutLα endonuclease assays (16) were carried out in a purified system composed of MutSβ (22 nM), MutLα (50 nM), RFC (15 nM), PCNA (100 nM), and an I/D heteroduplex or homoduplex DNA substrate (1.2 nM) at 37 °C for 10 min in a 20-μl reaction in the buffer described above. The reaction products were resolved on alkaline agarose

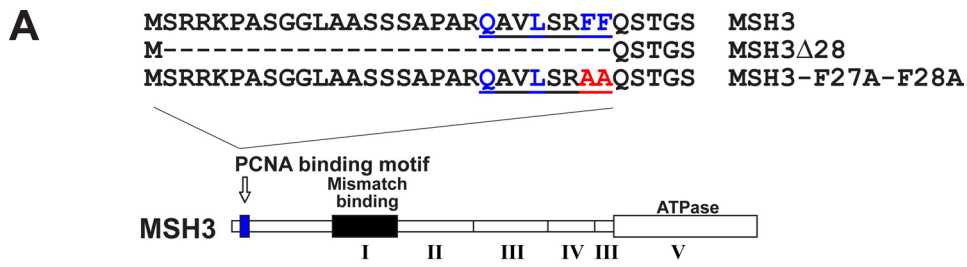

B

PCNA effects on affinity and specificity of dinucleotide loop recogntion by MutSβ

	K_D (nM)	
	200 bp -TG- I/D	200 bp-A•T
MutSβ	4 ± 1	39 ± 10
MutSβΔ28	4 ± 1	45 ± 8
MutSβ-F27A-F28A	2 ± 1	30 ± 12
MutSβ (+ 2μM PCNA)	5 ± 1	29 ± 8

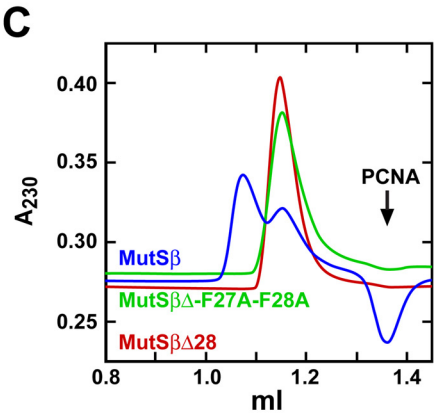

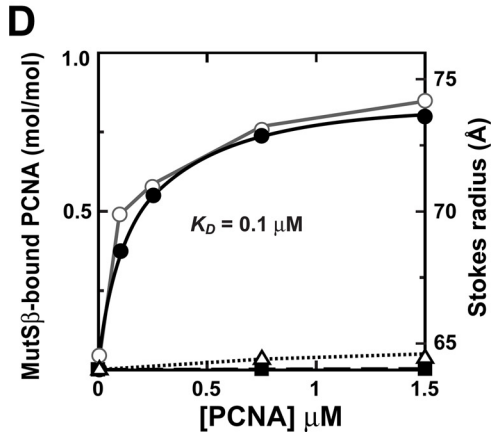

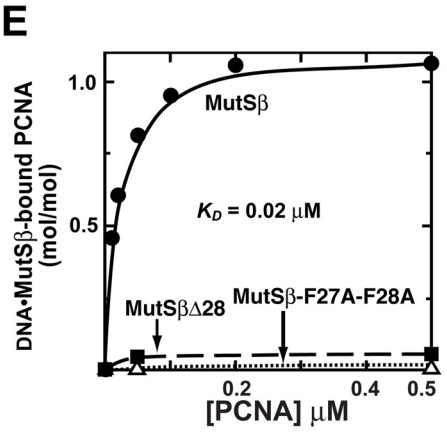

FIGURE 1. **Formation of a 1:1 equilibrium complex between MutSβ and PCNA is mediated by a PCNA-binding motif near the N terminus of MSH3.** *A*, domain structure of human MSH3 as predicted by sequence alignment with MSH6. The PCNA-binding motif (conserved residues shown in *blue*) near the N terminus of full-length MSH3 is deleted in MSH3Δ28 and altered by Ala substitution for the conserved Phe residues in MSH3-F27A-F28A. *B*, DNA affinities of MutSβ, MutSβΔ28, and MutSβ-F27A-F28A were determined by SPRS ("Experimental Procedures") by flowing the proteins over a sensor chip derivatized with a 200-bp homoduplex or a -TG- I/D heteroduplex DNA. Mass response units at saturation were recorded as a function of MutSβ concentration and fit to a rectangular hyperbola to yield apparent affinities shown. PCNA effects on MutSβ-DNA interaction were assessed by titration with MutSβ in the presence of 2.0 μM PCNA. *C*, interaction of PCNA with MutSβ in the absence of DNA was evaluated by equilibrium gel filtration ("Experimental Procedures"). Ten-μl samples containing 1 μM MutSβ (or 1.14 μM MutSβΔ28 or 1.0 μM MutSβ-F27A-F28A) and 0.75 μM PCNA were loaded onto a 2.4-ml Superdex 200 column equilibrated with 0.75 μM PCNA, and the column was developed isocratically at 0.01 ml/min. The protein elution profiles as detected by absorbance at 230 nm are shown for MutSβ (*blue*), MutSβΔ28 (*red*), and MutSβ-F27A-F28A (*green*). *D*, extents of PCNA trimer binding to MutSβ (*closed circles*), MutSβΔ28 (*closed squares*), or MutSβ-F27A-F28A (*open triangles*) were determined from trough areas as a function of free PCNA concentration. Binding isotherms shown were determined by nonlinear least squares fit to a rectangular hyperbola, which yielded a K_d of 0.10 μM and a stoichiometry of 0.8 PCNA homotrimer/wild type MutSβ heterodimer. Formation of the MutSβ-PCNA complex is associated with an increase in apparent Stokes radius (*open circles*). *E*, interaction parameters of PCNA with DNA-bound MutSβ were determined by SPRS. Solutions containing 0.10 μM MutSβ (or MutSβΔ28 or MutSβ-F27A-F28A) and 0–0.50 μM PCNA were allowed to flow over a sensor chip derivatized with a 200-bp -TG- I/D heteroduplex. The amount of PCNA bound to the sensor surface was determined as a function of PCNA concentration for MutSβ (*circles*), MutSβΔ28 (*squares*), or MutSβ-F27A-F28A (*open triangles*) by subtracting the mass response units recorded for each MutSβ variant alone from that determined in the presence of PCNA. Molar stoichiometries were calculated assuming that 1 response unit of MutSβ (232 kDa) corresponds to 0.37 response unit for the PCNA trimer (86 kDa). The data were fit to a rectangular hyperbola, yielding an apparent K_d of 0.02 μM, and a stoichiometry of 1 mol of PCNA/mol of MutSβ.

gels, and the extent of MutLα-catalyzed incision was measured by indirect end labeling (16).

RESULTS

MutSβ and PCNA Form a High Affinity 1:1 Complex—MutSβ interacts with PCNA via a conserved Q*XX*(L/I)*XX*FF motif that resides near the N terminus of MSH3 (23, 24, 26), but the molecular nature of the MutSβ-PCNA complex has not been examined. To address the nature of this interaction as well as the functional consequences of its disruption, we constructed MSH3 variants in which the PCNA-binding motif (PIP box) was either deleted (MSH3Δ28) or altered by amino acid substitution mutation (MSH3-F27A-F28A) (Fig. 1*A*). These variants were co-expressed with MSH2 and purified as stable heterodimers referred to as MutSβΔ28 and MutSβ-F27A-F28A. Both mutant heterodimers display Stokes radii comparable with the wild type protein as determined by gel filtration chromatography (Table 1). To determine whether these MSH3 mutations altered the mismatch recognition activity of MutSβ, we used SPRS to measure affinities of MutSβ, MutSβΔ28, and MutSβ-F27A-F28A for a 200-bp -TG- dinucleotide I/D heteroduplex or an otherwise identical homoduplex. The apparent affinities and specificities of the MutSβ variants did not differ significantly from that obtained with the wild type protein (Fig. 1*B*). Furthermore, wild type and mutant forms of MutSβ dissociated with similar kinetics from heteroduplex DNA upon ATP challenge (not shown). The presence of 2.0 μM PCNA, a saturating concentration for MutSβ-PCNA complex formation (see below), did not significantly alter the affinity or specificity of MutSβ interaction with heteroduplex/homoduplex DNA (Fig. 1*B*).

The MutSβ-PCNA complex was characterized by the Hummel-Dreyer equilibrium gel filtration procedure that was previously employed to determine equilibrium parameters that govern formation of the

TABLE 1

Biophysical properties of MutSβ and MutSβ-PCNA derived from SAXS and gel filtration

The radii of gyration (R_g) were determined from Guinier plots (supplemental Fig. S2*A*, *inset*) (32) in which SAXS data collected over a range of protein concentration (supplemental Fig. S2*C*) were extrapolated to zero concentration. The maximum particle dimension (D_{max}) was estimated from the $P(r)$ plots (49) shown in Fig. 5*A*. The Stokes radii were determined by gel filtration ("Experimental Procedures"). See also supplemental Fig. S2.

Sample	Molecular mass	SAXS				Gel filtration (Stokes radius)
		Calculated R_g	Guinier R_g	$P(r)$ R_g	D_{max}	
	kDa	*Å*	*Å*	*Å*	*Å*	*Å*
MutSβ	232		52 ± 0.2	49 ± 0.1	165	64
MutSβΔ28	229		50 ± 0.5	48 ± 0.1	160	64
MutSβ-F27A-F28A	232					64
PCNA[a]	86	34	33 ± 0.1	34 ± 0.1	92	40
MutSβ + PCNA (1:1)	318		67 ± 1	65 ± 0.2	220	74
MutSβΔ28+ PCNA (1:1)			50 ± 0.4			

[a] The data for PCNA are reproduced from the work of Iyer *et al.* (21).

MutSα-PCNA complex (21). The Hummel-Dreyer elution profile for MutSβ (Fig. 1*C*) in the presence of 0.75 μM PCNA shows two distinct but overlapping peaks followed by a trough at ~1.35 ml that represents depletion of PCNA from the running buffer caused by complex formation with MutSβ. Because the later eluting peak (1.14 ml) corresponds to free MutSβ, we infer that the earlier peak (1.1 ml) represents the MutSβ-PCNA complex. By contrast, MutSβΔ28 and MutSβ-F27A-F28A elute as single peaks (1.14 ml) corresponding to uncomplexed MutSβ. Furthermore, as judged by absence of a significant trough at 1.35 ml, the two mutant heterodimers fail to deplete PCNA from the equilibrating buffer, indicating that their ability to bind PCNA has been severely compromised. The extent of PCNA binding to MutSβ was a hyperbolic function of PCNA concentration corresponding to an apparent K_d of 0.10 μM and a stoichiometry of 0.9 PCNA trimer/MutSβ heterodimer (Fig. 1*D*). The formation of a complex with PCNA increases the Stokes radius of MutSβ from 64 to 74 Å (Table 1).

PCNA binding to DNA-bound MutSβ was evaluated by SPRS. As determined by this procedure, DNA-bound MutSβ interacts with PCNA with an apparent K_d of 0.020 μM and a stoichiometry of 1.1 mol of PCNA trimer/mol of MutSβ heterodimer (Fig. 1*C*). Although MutSβΔ28 and MutSβ-F27A-F28A efficiently bind heteroduplex DNA (Fig. 1*B*), PCNA interaction with the heteroduplex-bound mutant proteins was almost undetectable (Fig. 1*E*). The apparent affinity of PCNA for DNA-bound MutSβ as judged by SPRS is ~5-fold higher than that for free MutSβ as determined by the Hummel-Dreyer method. A similar difference has been observed for affinities of the MutSα-PCNA complex determined by the two methods (21) and is likely due to avidity or rebinding artifacts that are known to occur when multivalent species such as PCNA are present in the mobile phase of SPRS analysis (34).

MutSβ PIP Box Mutants Are Defective in MutLα Interaction—Interaction between MutS and MutL homologs has been documented in several systems (3, 4), but the nature of the human MutLα-MutSβ complex has not been addressed. We have therefore used SPRS to examine the capacity of MutSβ and its PIP box mutants to support formation of a MutLα-MutSβ-DNA ternary complex. As shown in Fig. 2*A*, in the presence of ATP-Mg^{+2} MutSβ forms specific but short-lived complexes with the 200-bp -TG- I/D heteroduplex described above. Inclusion of both MutLα and MutSβ resulted in a substantial increase in DNA-bound mass (Fig. 2*A*), indicative of ternary complex formation. This mass increase was not observed in the absence of ATP (not shown), and we were unable to detect DNA binding by MutLα alone (not shown). The latter results are consistent with previous findings that assembly of ternary complexes involving MutL and MutS homologs is ATP-dependent and that DNA binding by MutL homologs is limited at physiological ionic strength (17, 25, 35–38). The lifetime of the ternary complex is also short, with 80% dissociating with a $t_{1/2}$ of 7 s. The apparent affinity of MutLα for DNA-bound MutSβ was estimated from the MutLα dependence of the mass increase over and above that observed with MutSβ alone (0.1 μM). As shown in Fig. 2*B*, the results fit well to a rectangular hyperbola with a K_d of 0.4 μM.

To our surprise, substitution of MutSβΔ28 or MutSβ-F27A-F28A (Fig. 2*A*, *middle* and *bottom panels*) for MutSβ abolished ternary complex formation, indicating that MSH3 PIP box mutations compromise the ability of DNA-bound MutSβ to interact with MutLα. By contrast, deletion of the PIP box motif of MutSα, although severely attenuating the capacity of MutSα to associate with PCNA (21), does not alter the ability of the MSH2-MSH6 heterodimer to support ternary complex formation with MutLα and heteroduplex DNA (supplemental Fig. S1).

To assess the interaction of MutSβ with MutLα by an independent method, we employed far Western analyses wherein proteins applied to a nitrocellulose membrane were incubated with PCNA or MutLα in solution, followed by immunochemical detection of membrane-bound PCNA or MutLα. As shown in Fig. 2*C* (*top panel*), complexes of PCNA with MutSα, MutSβ, and MutLα can be detected by this method, confirming previous findings (14, 26). However, binding of PCNA to MutSβΔ28 and MutSβ-F27A-F28A to PCNA was substantially reduced compared that of wild type MutSβ. When MutLα was in solution (Fig. 2*C*, *bottom panel*), robust complex formation with membrane-bound MutSβ was observed. However, binding of MutLα to both MutSβΔ28 and MutSβ-F27A-F28A was severely compromised. Although PCNA in solution is able to associate with membrane-bound MutLα, such an interaction was not observed in the converse experiment wherein MutLα was in solution and PCNA was membrane-bound. The reason for this difference is not clear, but it is possible that PCNA binding to the membrane may occlude access to its MutLα-binding surface. An alternate possibility is that the α-MLH1 antibody used to probe for presence of PCNA-bound MutLα may compete with PCNA for a common binding site. MutLα in solution also interacts poorly with nitrocellulose-bound MutSα, possibly because of membrane occlusion effects. Taken

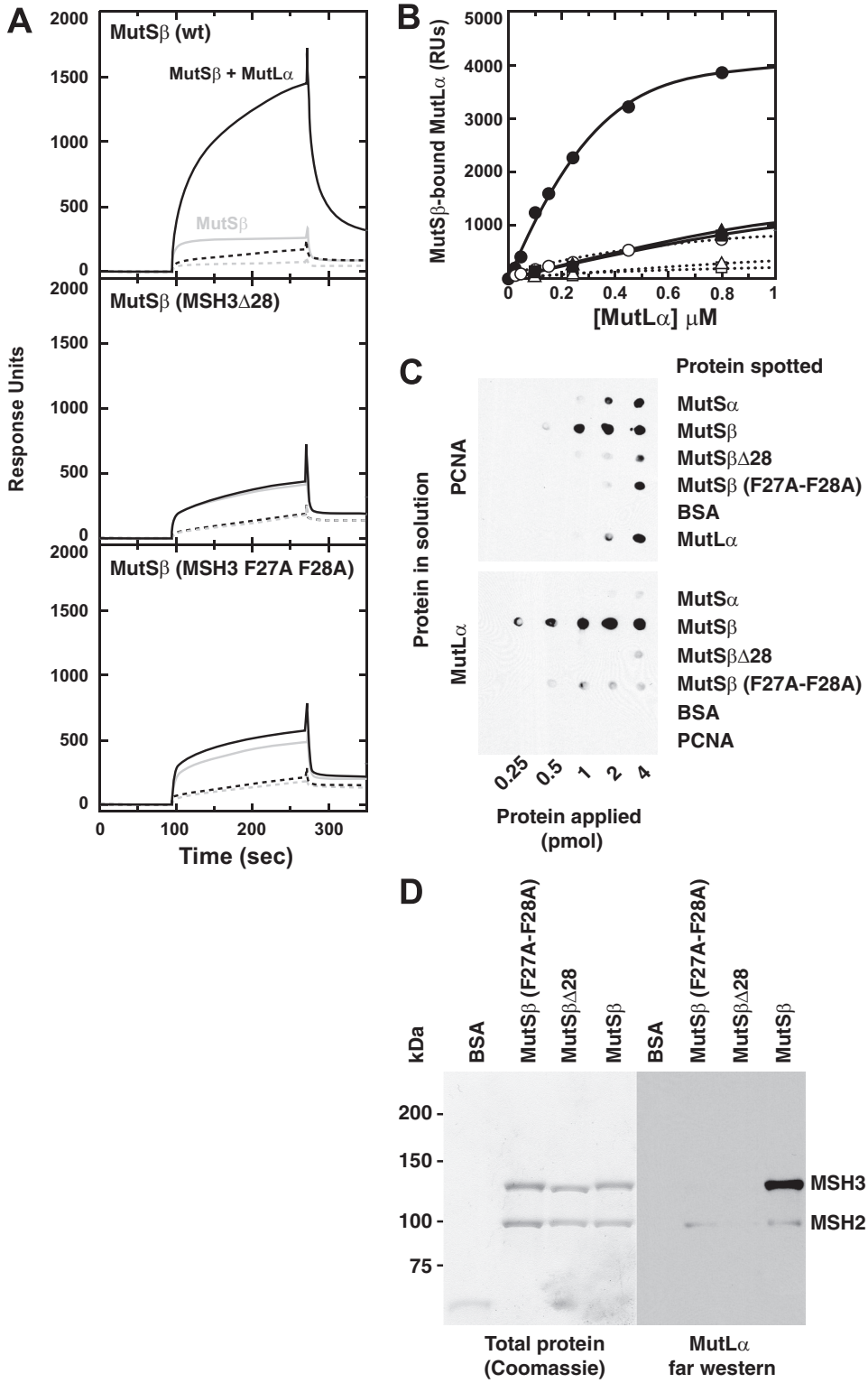

FIGURE 2. **MutSβ PIP box mutants are defective in MutLα interaction.** *A*, ATP-dependent assembly of the MutLα-MutSβ-DNA ternary complex was scored by SPRS using a 200 bp -TG- I/D heteroduplex (*solid lines*) or homoduplex (*dashed lines*) DNA. The *top panel* shows mass bound upon flow of 0.10 μM MutSβ alone (*gray*) or a mixture of 0.10 μM MutSβ and 0.24 μM MutLα (*black*) over heteroduplex or homoduplex in the presence of 1 mM ATP. Similar analyses were performed with MutSβΔ28 (*middle panel*) and MutSβ-F27A-F28A. *B*, apparent affinity of MutLα for MutSβ (*circles*), MutSβΔ28 (*squares*), or MutSβ-F27A-F28A (*triangles*) was determined from SPRS experiments like those described above but in which the concentration of MutLα was varied as shown in the presence of 0.10 μM MutSβ. The data were fit to a hyperbola by nonlinear least squares regression to yield an apparent K_d of 0.40 μM on heterduplex DNA (*closed symbols*). Complex formation on homoduplex DNA (*open symbols*) was not saturable. *C*, interaction of MutSβ variants with PCNA and MutLα was also assessed independently by far Western analysis ("Experimental Procedures"). The indicated amount of each protein was spotted on a nitrocellulose membrane and incubated with 0.18 μM of either PCNA or MutLα at 4 °C overnight. PCNA and MutLα were detected immunochemically. *D*, interaction of MutLα with separated MSH2 or MSH3 subunits of MutSβ or its variants (bovine serum albumin (*BSA*) served as a negative control) was assayed by far Western analysis after subunit resolution by SDS-PAGE ("Experimental Procedures"). The membrane treatment was as in *C* except that incubation was with 0.09 μM of MutLα. See also supplemental Fig. S1.

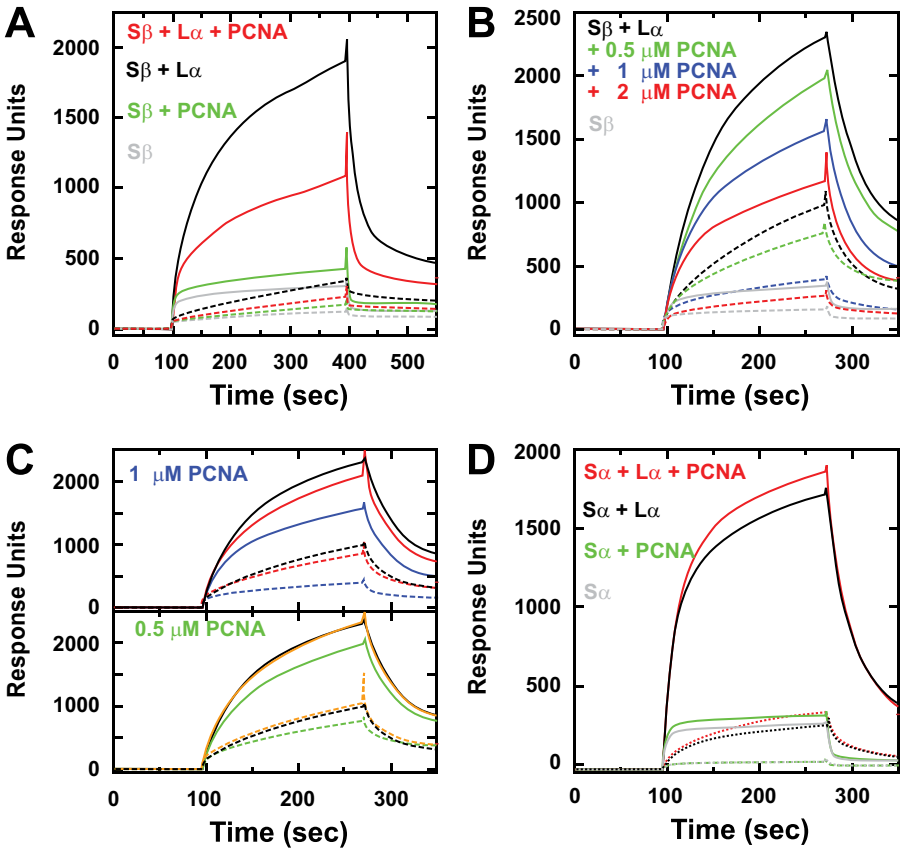

FIGURE 3. **PCNA and MutLα compete for binding to MutSβ but not to MutSα.** The effect of PCNA on formation of DNA-MutSβ-MutLα and DNA-MutSα-MutLα ternary complexes was evaluated by SPRS using a sensor chip derivatized with 200-bp -TG- I/D heteroduplex (*solid lines*) or control homoduplex (*dashed lines*) DNA. *A*, sensorgram profiles show mass response units upon flow of solutions containing 1 mM ATP and 0.10 μM MutSβ (*gray*); 0.10 μM MutSβ and 0.24 μM MutLα (*black*); 0.10 μM MutSβ and 2.0 μM PCNA (*green*); and 0.10 μM MutSβ, 0.24 μM MutLα and 2.0 μM PCNA (*red*). *B*, inhibition of ternary complex formation as a function of PCNA concentration was measured by monitoring mass bound when solutions containing 0.050 μM MutSβ (*gray*) or a mixture composed of 0.050 μM MutSβ, 0.050 μM MutLα, and one of the following were allowed to flow over the sensor chip in the presence of 0.25 mM ATP and 125 mM KCl: 0 (*black*), 0.50 (*green*), 1.0 (*blue*), or 2.0 (*red*) μM PCNA. *C*, effect of p21 on PCNA-dependent inhibition of DNA-MutSβ-MutLα ternary complex formation was assessed as in *B* by flowing a mixture of 0.050 μM MutSβ, 0.050 μM MutLα, and 0.25 mM ATP (*black*) or the same mixture supplemented with one of the following: 1.0 μM PCNA (*blue*), 0.50 μM PCNA (*green*), 1.0 μM PCNA and 6.0 μM p21 (*red*), or 0.50 μM PCNA and 6.0 μM p21 (*orange*). *D*, SPRS experiments were as in *A* but with 0.20 μM MutSα (*gray*); 0.20 μM MutSα and 0.20 μM MutLα (*black*); 0.20 μM MutSα and 1.6 μM PCNA (*green*); and 0.20 μM MutSα, 0.20 μM MutLα and 1.6 μM PCNA (*red*).

together with the SPRS ternary complex observations described above, these far Western results indicate that the MutSβ motif responsible for its interaction, MutLα, resides at least in part within the N-terminal 28 residues of MSH3 and includes Phe-27 and Phe-28. In fact, strong MutLα interaction with the MSH3 subunit of MutSβ was directly demonstrable by far Western analysis of membrane transfers from SDS gel-resolved MutSβ subunits, and this interaction was abolished by the PIP box mutations described above (Fig. 2*D*).

PCNA Competes with MutLα for Binding to MutSβ but Not to MutSα—The simplest interpretation of these findings is overlap of MSH3 binding sites for PCNA and MutLα, an idea that predicts competition of the two proteins for complex formation with MutSβ. To test this possibility, we used SPRS to examine effects of PCNA on DNA-MutSβ-MutLα ternary complex formation. The addition of 2.0 μM PCNA to a solution containing MutSβ results in an increase in mass bound to the sensor surface consistent with MutSβ-PCNA complex formation (Fig. 3*A*, compare *gray* and *green lines*). The addition of the same amount of PCNA to a mixture of MutSβ and MutLα results in a substantial decrease in chip-bound mass as compared with that in the absence of the clamp (Fig. 3*A*, compare *red* and *black lines*), indicating that PCNA inhibits the assembly of the DNA-MutSβ-MutLα ternary complex. PCNA inhibition of this reaction increases with increasing PCNA concentration (Fig. 3*B*), an effect that is reversed by the presence of a molar excess of the PCNA-binding cell cycle regulator $p21^{CIP1}$ (Fig. 3*C*).

As discussed above, unlike MutSβ PIP box mutants, MutSαΔ12, which lacks the MSH6 PCNA interaction motif, is proficient in assembly of the DNA-MutSα-MutLα ternary complex (supplemental Fig. S1). It might therefore be expected that assembly of the MutSα ternary complex would be refractory to the inhibitory effect of PCNA. Indeed, the presence of PCNA in solutions containing MutSα, MutLα, and ATP resulted in a further increase in DNA-bound mass (Fig. 3*D*, compare *red* and *black lines*), indicating the formation of a DNA-MutSα-PCNA-MutLα quarternary complex. Interestingly, the resultant mass increase is ~2–3-fold greater than that caused by PCNA association with the DNA-MutSα complex, which may indicate that MutLα promotes multiple MutSα loading events or that PCNA may interact with both the MutSα and MutLα components of the ternary complex (Fig. 2*C*) (13). By contrast, MutSαΔ12 fails to support formation of a DNA-MutSαΔ12-PCNA-MutLα quarternary complex (not shown), indicating that initial association of PCNA with the DNA-MutSα-MutLα ternary complex occurs via multiply loaded MutSα molecules. These data suggest that in contrast to MutSβ, MutSα has distinct binding sites that can be simultaneously occupied by MutLα and PCNA.

The MSH3 PIP Box Is Required for MutLα Endonuclease Activation and Bidirectional Mismatch-provoked Excision and Repair—We have previously shown that MutSαΔ12, although unable to associate with PCNA, retains mismatch recognition activity, supports MutLα endonuclease activation, and is as active as the wild type protein in mismatch-provoked excision. The mutant does, however, display a partial defect in 5′- but not 3′-directed mismatch repair (21). To determine the functional consequences of disruption of the MSH3 PIP box motif in MutSβ, we examined the activities of MutSβ PIP box mutants

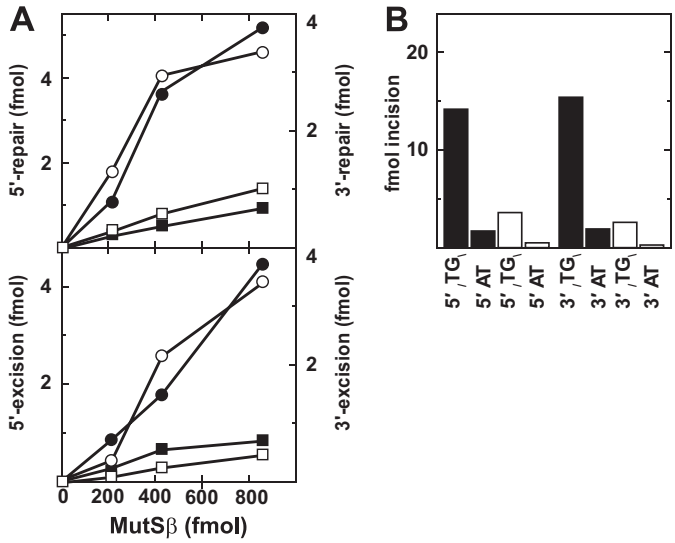

FIGURE 4. **MSH3 PIP box mutants are defective in MutLα endonuclease activation, mismatch-provoked excision, and mismatch repair.** *A*, *top panel*, repair of 5′- (*closed symbols*) or 3′-dinucleotide (*open symbols*) I/D heteroduplex ("Experimental Procedures") was scored in nuclear extracts of *MSH2*$^{-/-}$ RL95-2 cells as a function of exogenously added MutSβ (*circles*) or MutSβΔ28 (*squares*). *Bottom panel*, excision on 5′- and 3′- substrates was scored by NheI-resistant gap formation assay (33) in RL95-2 extracts in the absence of exogenous dNTPs as a function of added MutSβ and MutSβΔ28. *B*, MutSβ (*black bars*) and MutSβΔ28 (*white bars*) (100 ng or 430 fmol) were compared for their ability to support MutLα endonuclease activation (16) on 5′ and 3′ -TG- I/D heteroduplex or A-T homoduplex DNAs ("Experimental Procedures"). The results shown are corrected for background observed in the absence of MutSβ, MutLα, RFC, and PCNA.

in the nuclear extracts of MSH2$^{-/-}$ RL95-2 cells and in a purified system that scores MutLα endonuclease activation. As judged by extract assay, MutSβΔ28 displays a severe defect in 5′- and 3′-excision and repair as compared with the wild type protein (Fig. 4*A*). Unlike the wild type protein, the capacity of this truncation mutant to activate the MutLα endonuclease is also severely attenuated (Fig. 4*B*). The initial rates of MutSβ-dependent MutLα endonucleolytic activity supported by MutSβ-F27A-F28A are also ~3–4-fold lower than the wild type protein (data not shown). Thus, unlike MSH6, the integrity of the MSH3 PIP box is required for mismatch repair.

Solution Conformations of MutSβ and the MutSβ-PCNA Complex—Supplemental Fig. S2*A* shows solution x-ray scattering data and linear portions of Guinier plots for MutSβ, MutSβΔ28, PCNA, and an equimolar mixture of MutSβ and PCNA. The corresponding pairwise interatomic distances distributions ($P(r)$) were derived from scattering profiles by indirect Fourier transform (Fig. 5*A*). Table 1 summarizes the model-independent structural parameters R_g and D_{max} obtained from these experiments. As observed previously for MutSα (21), the $P(r)$ distributions for MutSβ and MutSβΔ28 are skewed toward larger r values, indicating that the conformations of these two heterodimers are significantly more elongated than the published structures of truncated forms of MutS homologs (supplemental Fig. S2*D*) (39, 40). The addition of one PCNA trimer equivalent to MutSβ results in a further skewing of the $P(r)$ distribution toward higher values.

As noted above (Table 1), gel filtration studies showed an increase in Stokes radius for MutSβ from 64 to 74 Å because of formation of the MutSβ-PCNA complex. The similar but distinct conformational parameter, R_g, measured by SAXS also increases when one PCNA equivalent is added to MutSβ, an effect that is not observed with MutSβΔ28 (Table 1). The SAXS data also permit extraction of forward scattering intensity $I(0)$, which is a linear function of molecular mass (41) (supplemental Fig. S2*B*). $I(0)$ values determined for 1:1 mixtures of the MutSβ and PCNA proteins are substantially greater than those for either of the individual molecules (supplemental Fig. S2*B*) and are consistent with an expected molecular mass of a 1:1 MutSβ-PCNA trimer complex (318 kDa). By contrast, an equimolar mixture of MutSβΔ28 and PCNA yields a significantly lower value for $I(0)$, indicating that the two proteins fail to interact (see below).

Given the trivalent nature of PCNA (42), it is potentially possible to assemble MutSβ-PCNA complexes of differing stoichiometries: MutSβ-PCNA, $(MutS\beta)_2$-PCNA, and $(MutS\beta)_3$-PCNA, with monovalent complexes favored under conditions of PCNA excess. As discussed above, the stoichiometry of this interaction determined by equilibrium gel filtration and SPRS is 1 MutSβ heterodimer/PCNA homotrimer. Because complex formation in both of these procedures was measured under conditions where PCNA was in excess, these experiments are insensitive to the formation of potential $(MutS\beta)_2$-PCNA and $(MutS\beta)_3$-PCNA assemblies. To address this issue, we determined $I(0)$ values for PCNA-MutSβ mixtures as a function of molar ratio under conditions where the concentration of each protein was well above the K_d for binary complex formation. As shown in Fig. 5*B*, the experimental maximum $I(0)$ occurs at a PCNA:MutSβ molar ratio of 0.5, indicative of the presence of multivalent species. Comparison of experimentally determined values with those calculated for mixtures of $(MutS\beta)_2$-PCNA and MutSβ-PCNA or $(MutS\beta)_3$-PCNA and MutSβ-PCNA demonstrated that the MutSβ-PCNA complex is the favored species at PCNA:MutSβ molar ratios ≥1, but as many as 20% of the complexes are multivalent at lower values (supplemental Table S1). Furthermore, $I(0)$ does not increase as a function of the MutSβΔ28:PCNA ratio (Fig. 5*B*), a finding that independently confirms the PCNA interaction defect of this MutSβ variant.

Ab Initio Shape Reconstructions for MutSβ and the MutSβ-PCNA Complex from SAXS Data—Model-independent D_{max} values (Table 1) (21) indicate that the MutSβ conformation in solution (D_{max} = 165 Å) is more extended than MutSαΔ341 (D_{max} = 140 Å) but more compact than MutSα (D_{max} = 202 Å). Because a crystal structure of MutSβ is not available, the SAXS results described above were used to generate low resolution conformational models (43) of the heterodimer, as well as its complex with PCNA. The validity of the models was assessed using the crystal structures of the human MutSαΔ341-DNA complex (40) and PCNA (42). *Ab initio* envelopes of MutSβ and MutSβΔ28 (Fig. 5*C*) accommodate superimposition of the crystal structure of the MutSαΔ341-DNA complex and display additional mass that presumably corresponds to portions of MutSβ that do not share sequence or conformational homology with MutSαΔ341.

As noted above, the addition of one trimer equivalent of PCNA to MutSβ results in a $P(r)$ plot that is skewed toward higher interatomic distances by ~ 55 Å, an effect that is mani-

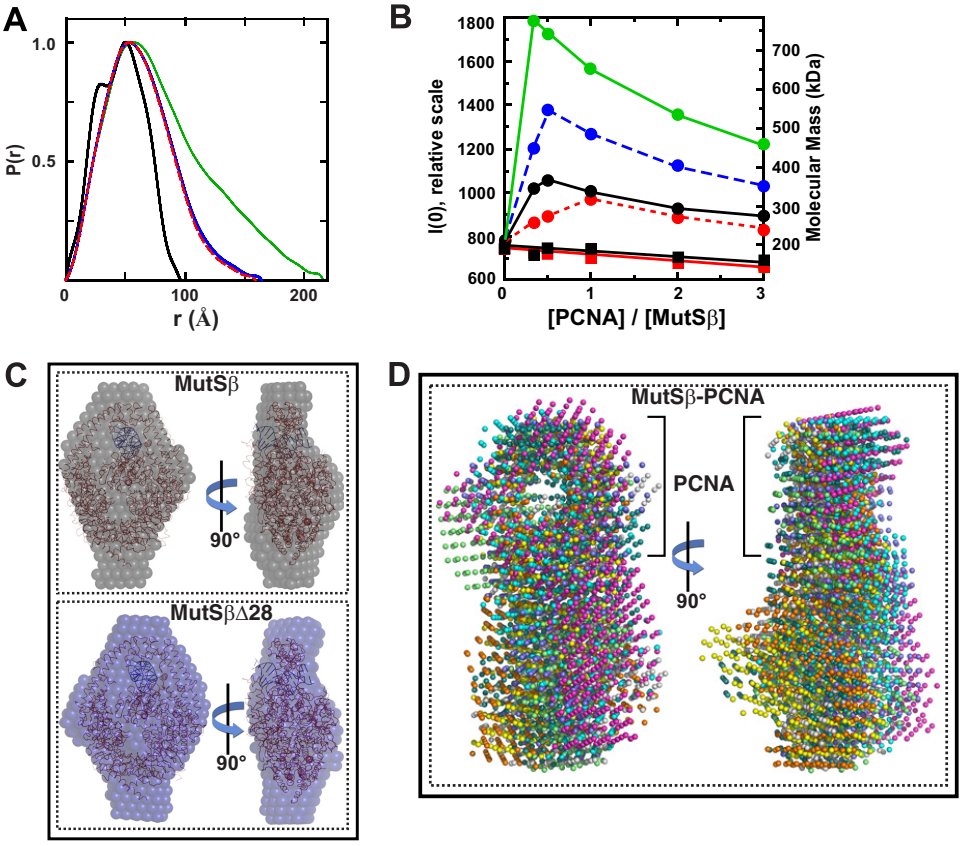

FIGURE 5. **Small angle x-ray scattering studies of MutSβ and the MutSβ-PCNA complex.** *A*, normalized pair distribution (*P*(*r*)) plots for MutSβ (*blue*), MutSβΔ28 (*red*), an equimolar mixture of MutSβ and PCNA (*green*), and PCNA alone (*black*, reproduced from Ref. 21) were derived by indirect Fourier transform (49) of solution scattering data (supplemental Fig. S2*A*). *B*, stoichiometry of the MutSβ-PCNA interaction was determined ("Experimental Procedures") from experimentally determined forward scattering intensities *I*(0) plotted as a function of PCNA:MutSβ (*black circles*) or PCNA:MutSβΔ28 (*black squares*) molar ratio. The theoretical dependence of *I*(0) on PCNA:MutSβ molar ratio was calculated for scenarios that assume formation of the stoichiometric complexes MutSβ-PCNA (318 kDa) (*red circles*), $(MutS\beta)_2$-PCNA (550 kDa) (*blue circles*), or $(MutS\beta)_3$-PCNA (782 kDa) (*green circles*) ("Experimental Procedures"). The expected *I*(0) values for PCNA mixtures with MutSβΔ28 (*red squares*) are also shown with the assumption of no interaction. Molecular masses corresponding to *I*(0) values (supplemental Fig. S2*B*) are indicated on the *right vertical axis*. *C*, *ab initio* shape reconstructions of MutSβ and MutSβΔ28 were performed from SAXS data as described (21). The envelopes shown represent an average of 10 independent shape reconstructions. Because of nonavailability of a MutSβ crystal structure, the MutSαΔ341-DNA complex structure (40) is superimposed on the MutSβ SAXS envelope for size reference. *D*, *ab initio* shapes of the MutSβ-PCNA complex were generated as described above from experimental scattering data collected for 1:1 molar mixtures of MutSβ and PCNA. Eight independent *ab initio* shapes in multiple colors are shown manually superimposed on each other. Despite the low resolution of these models, a central channel of dimensions similar to that of PCNA is clearly defined and was used to align the individual reconstructions. See also supplemental Fig. S2 and Table S1.

fested as a substantial increase in D_{max} (Fig. 5*A* and Table 1). However, the maximum *P*(*r*) value for the MutSβ-PCNA complex occurs at an *r* value (56 Å) that is nearly identical to that for MutSβ alone (54 Å). These results suggest that the MutSβ-PCNA complex adopts an "extended" end-to-end conformation rather than a stacked arrangement wherein the DNA-binding channels of the two proteins are juxtaposed, because the latter conformer would be expected to display a *P*(*r*) maximum at a substantially higher *r* value (21). In fact, *ab initio* shapes generated from SAXS data are consistent with an end-to-end association of MutSβ and PCNA (Fig. 5*D*), with the ring shape of PCNA being clearly defined in the low resolution models along with substantial associated mass consistent with presence of a MutS homolog dimer equivalent. By contrast to the variety of extended *ab initio* shapes obtained for the MutSα-PCNA complex (21), low resolution MutSβ-PCNA models are strikingly similar (Fig. 5*D*), suggesting that there is limited variability between individual MutSβ-PCNA conformers in solution.

DISCUSSION

Protein-protein interactions are thought to coordinate the sequence of molecular events involved in DNA mismatch repair. A number of multi-protein assemblies have been documented in this system including MutSα-PCNA, MutSβ-PCNA, MutSα-MutLα, MutSβ-MutLα, MutLα-PCNA, MutSα-ExoI, MutLα-ExoI, and ExoI-PCNA (1–5). Of these, the MutSα-PCNA complex has received the most attention in the literature, but recent studies indicate that this interaction plays only a limited role in the error correction reaction (20, 21, 23).

Because MSH3, like MSH6, interacts with PCNA via a PIP box located near its N terminus, it might be expected that the MutSβ-PCNA complex may display similar characteristics. However, our results indicate that this is not the case. The affinity of MutSβ for PCNA is ~8-fold higher than that of MutSα, a difference that may be necessitated by the fact that the MutSβ levels in human cells are 5–8-fold lower than that of the MSH2-MSH6 heterodimer (30, 44). Furthermore, although the stoichiometry of the MutSα-PCNA complex is limited to 1:1 even when MutSα is in molar excess (21), as much as 20% of the MutSβ-PCNA complexes are multivalent under conditions of MutSβ excess. This valency difference could reflect steric factors in that MutSβ is significantly smaller than MutSα. Despite these differences, complex formation between MutSβ and PCNA does not significantly alter the affinity or specificity of MutSβ for a -TG- insert, a property it shares with MutSα.

However, the most striking difference between MutSβ and MutSα is the finding described here that the modes of interaction of the two mismatch recognition activities with PCNA and MutLα differ dramatically. In contrast to MutSα, which can interact independently with PCNA and MutLα, interaction of these two proteins with MutSβ occurs in an either/or fashion. As discussed above, MSH3 PIP box mutations compromise MutSβ interaction with both PCNA and MutLα. Furthermore, PCNA competes with MutLα for binding to MutSβ and inhibits ATP-dependent assembly of the DNA-MutSβ-MutLα ternary complex, an effect that is reversed by p21, which is known to

interact strongly with PCNA (45). The simplest interpretation of these results is that the MutSβ motif(s) involved in its interaction with MutLα partially overlap with the MSH3 PIP box responsible for the MutSβ-PCNA interaction. It is noteworthy in this regard that an RS(K/R)(Y/F)F peptide has been identified as a MutLα interaction motif in human Exo1 and BLM helicase (46). A similar highly conserved motif, LSRFF, overlaps with the MSH3 PIP box (QAVLSRFF) and may correspond to one component of the MutLα-binding site within MutSβ. To our knowledge, this is the first instance where residues within the PCNA-binding motif of a protein are also employed for interaction with a second activity.

Recently, Fishel and co-workers (47) have described an interaction between human MLH1 and a polypeptide corresponding to the N-terminal 250 residues of human MSH3; interaction of MLH1 with MSH2 was not observed in this study. These findings are consistent with those described here. By contrast, studies in *Saccharomyces cerevisiae* (48) have implicated yMSH2 residues in the interaction of yMutSα with yMutLα, although mutational alteration of the yMSH2 residues in question did not result in an interaction defect as severe as that described in our study. It is thus conceivable that MSH2 sequence elements contribute to MutSβ-MutLα interaction, but if this is the case, residues in the vicinity of the MSH3 PIP box must also be required.

Our finding that PCNA and MutLα interact in an either/or fashion with MutSβ may reflect steric interference effects but could also be indicative of use of common interaction interfaces. For example, MutSβ and MutLα interaction with a common PCNA motif would account for our findings, as would MutSβ and PCNA interaction with a common interface on MutLα.

Because ATP-dependent assembly of a ternary complex involving heteroduplex DNA and a MutS and MutL homolog is believed to be a key step in the initiation of mismatch repair (3, 4), the inability of MutSβ PIP box mutants to support MutLα endonuclease activation, mismatch-provoked excision, and repair might be attributed to the inability of these mutants to support ternary complex formation. However, it is also possible that in contrast to the MutSα-initiated reaction, MutSβ interaction with PCNA may be a key step in MutSβ-initiated repair events. The pleiotropic nature of these mutants does not permit distinction between these possibilities, although our results almost certainly indicate that MutSα- and MutSβ-initiated mismatch repair events proceed by distinct mechanisms.

Interestingly, *S. cerevisiae* studies have suggested that although PIP box integrity may be required for MSH3 function, it has only a limited role in MSH6 activity (20, 23). In an *msh3* null background, the rate of frameshift mutagenesis within a A_{14}:T_{14} run was ~ 30-fold higher for an *msh6*Δ allele (1.5×10^{-3}) than for a *msh6* PIP box mutant (5.2×10^{-5}) (23). By contrast, deletion of *msh3* in an *msh6* null background resulted in a mutation rate (1.5×10^{-3}) only ~2–3-fold higher than that observed upon inactivation of the MSH3 PIP box (6.5×10^{-4}) (23). Our findings that MSH3 PIP box mutations are pleiotropic may explain these observations.

A potential mechanistic implication of our findings is that whereas PCNA is required for both MutSα- and MutSβ-dependent activation of MutLα endonuclease, a transient increase in local PCNA concentration could lead to specific destabilization of the MutLα-MutSβ-DNA complex, thus aborting a MutSβ-initiated event to allow a MutSα-dependent reaction to proceed unhindered. Because some I/D mispairs are subject to either MutSα- or MutSβ-dependent repair (30), this type of PCNA-mediated switch might function to control processing of such lesions by a particular pathway.

Acknowledgments—We thank Celia Baitinger for assistance with DNA substrate preparation and Leonid Dzantiev for helpful discussions.

REFERENCES

1. Kolodner, R. D., and Marsischky, G. T. (1999) *Curr. Opin. Genet. Dev.* **9,** 89–96
2. Kunkel, T. A., and Erie, D. A. (2005) *Annu. Rev. Biochem.* **74,** 681–710
3. Iyer, R. R., Pluciennik, A., Burdett, V., and Modrich, P. L. (2006) *Chem. Rev.* **106,** 302–323
4. Hsieh, P., and Yamane, K. (2008) *Mech. Ageing Dev.* **129,** 391–407
5. Li, G. M. (2008) *Cell Res.* **18,** 85–98
6. Peltomäki, P. (2003) *J. Clin. Oncol.* **21,** 1174–1179
7. Stojic, L., Brun, R., and Jiricny, J. (2004) *DNA Repair* **3,** 1091–1101
8. Zhang, N., Lu, X., Zhang, X., Peterson, C. A., and Legerski, R. J. (2002) *Mol. Cell. Biol.* **22,** 2388–2397
9. Zhao, J., Jain, A., Iyer, R. R., Modrich, P. L., and Vasquez, K. M. (2009) *Nucleic Acids Res.* **37,** 4420–4429
10. Di Noia, J. M., and Neuberger, M. S. (2007) *Annu. Rev. Biochem.* **76,** 1–22
11. Brouwer, J. R., Willemsen, R., and Oostra, B. A. (2009) *BioEssays* **31,** 71–83
12. Genschel, J., and Modrich, P. (2003) *Mol. Cell* **12,** 1077–1086
13. Dzantiev, L., Constantin, N., Genschel, J., Iyer, R. R., Burgers, P. M., and Modrich, P. (2004) *Mol. Cell* **15,** 31–41
14. Constantin, N., Dzantiev, L., Kadyrov, F. A., and Modrich, P. (2005) *J. Biol. Chem.* **280,** 39752–39761
15. Zhang, Y., Yuan, F., Presnell, S. R., Tian, K., Gao, Y., Tomkinson, A. E., Gu, L., and Li, G. M. (2005) *Cell* **122,** 693–705
16. Kadyrov, F. A., Dzantiev, L., Constantin, N., and Modrich, P. (2006) *Cell* **126,** 297–308
17. Blackwell, L. J., Wang, S., and Modrich, P. (2001) *J. Biol. Chem.* **276,** 33233–33240
18. Räschle, M., Dufner, P., Marra, G., and Jiricny, J. (2002) *J. Biol. Chem.* **277,** 21810–21820
19. Mendillo, M. L., Mazur, D. J., and Kolodner, R. D. (2005) *J. Biol. Chem.* **280,** 22245–22257
20. Flores-Rozas, H., Clark, D., and Kolodner, R. D. (2000) *Nat. Genet.* **26,** 375–378
21. Iyer, R. R., Pohlhaus, T. J., Chen, S., Hura, G. L., Dzantiev, L., Beese, L. S., and Modrich, P. (2008) *J. Biol. Chem.* **283,** 13310–13319
22. Plotz, G., Welsch, C., Giron-Monzon, L., Friedhoff, P., Albrecht, M., Piiper, A., Biondi, R. M., Lengauer, T., Zeuzem, S., and Raedle, J. (2006) *Nucleic Acids Res.* **34,** 6574–6586
23. Clark, A. B., Valle, F., Drotschmann, K., Gary, R. K., and Kunkel, T. A. (2000) *J. Biol. Chem.* **275,** 36498–36501
24. Johnson, R. E., Kovvali, G. K., Guzder, S. N., Amin, N. S., Holm, C., Habraken, Y., Sung, P., Prakash, L., and Prakash, S. (1996) *J. Biol. Chem.* **271,** 27987–27990
25. Habraken, Y., Sung, P., Prakash, L., and Prakash, S. (1997) *Curr. Biol.* **7,** 790–793
26. Kleczkowska, H. E., Marra, G., Lettieri, T., and Jiricny, J. (2001) *Genes Dev.* **15,** 724–736
27. Parsons, R., Li, G. M., Longley, M. J., Fang, W. H., Papadopoulos, N., Jen, J., de la Chapelle, A., Kinzler, K. W., Vogelstein, B., and Modrich, P. (1993) *Cell* **75,** 1227–1236
28. Genschel, J., and Modrich, P. (2009) *J. Biol. Chem.* **284,** 21536–21544
29. Blackwell, L. J., Bjornson, K. P., and Modrich, P. (1998) *J. Biol. Chem.* **273,**

32049–32054
30. Genschel, J., Littman, S. J., Drummond, J. T., and Modrich, P. (1998) *J. Biol. Chem.* **273,** 19895–19901
31. Gill, S. C., and von Hippel, P. H. (1989) *Anal. Biochem.* **182,** 319–326
32. Guinier, A., and Fournet, G. (1955) *Small-angle Scattering of X-rays*, John Wiley & Sons, Inc., New York
33. Genschel, J., and Modrich, P. (2006) *Methods Enzymol.* **408,** 273–284
34. Myszka, D. G. (1999) *J. Mol. Recognit.* **12,** 279–284
35. Grilley, M., Welsh, K. M., Su, S. S., and Modrich, P. (1989) *J. Biol. Chem.* **264,** 1000–1004
36. Habraken, Y., Sung, P., Prakash, L., and Prakash, S. (1998) *J. Biol. Chem.* **273,** 9837–9841
37. Gu, L., Hong, Y., McCulloch, S., Watanabe, H., and Li, G. M. (1998) *Nucleic Acids Res.* **26,** 1173–1178
38. Galio, L., Bouquet, C., and Brooks, P. (1999) *Nucleic Acids Res.* **27,** 2325–2331
39. Lamers, M. H., Perrakis, A., Enzlin, J. H., Winterwerp, H. H., de Wind, N., and Sixma, T. K. (2000) *Nature* **407,** 711–717
40. Warren, J. J., Pohlhaus, T. J., Changela, A., Iyer, R. R., Modrich, P. L., and Beese, L. S. (2007) *Mol. Cell* **26,** 579–592
41. Kratky, O. (1963) *Prog. Biophys. Biophys. Chem.* **13,** 105–173
42. Kontopidis, G., Wu, S. Y., Zheleva, D. I., Taylor, P., McInnes, C., Lane, D. P., Fischer, P. M., and Walkinshaw, M. D. (2005) *Proc. Natl. Acad. Sci. U.S.A.* **102,** 1871–1876
43. Svergun, D. I., Petoukhov, M. V., and Koch, M. H. (2001) *Biophys. J.* **80,** 2946–2953
44. Drummond, J. T., Genschel, J., Wolf, E., and Modrich, P. (1997) *Proc. Natl. Acad. Sci. U.S.A.* **94,** 10144–10149
45. Flores-Rozas, H., Kelman, Z., Dean, F. B., Pan, Z. Q., Harper, J. W., Elledge, S. J., O'Donnell, M., and Hurwitz, J. (1994) *Proc. Natl. Acad. Sci. U.S.A.* **91,** 8655–8659
46. Dherin, C., Gueneau, E., Francin, M., Nunez, M., Miron, S., Liberti, S. E., Rasmussen, L. J., Zinn-Justin, S., Gilquin, B., Charbonnier, J. B., and Boiteux, S. (2009) *Mol. Cell Biol.* **29,** 907–918
47. Charbonneau, N., Amunugama, R., Schmutte, C., Yoder, K., and Fishel, R. (2009) *Cancer Biol. Ther.* **8,** 1411–1420
48. Mendillo, M. L., Hargreaves, V. V., Jamison, J. W., Mo, A. O., Li, S., Putnam, C. D., Woods, V. L., Jr., and Kolodner, R. D. (2009) *Proc. Natl. Acad. Sci. U.S.A.* **106,** 22223–22228
49. Svergun, D. I. (1992) *J. Appl. Crystallogr.* **25,** 495–503